Prominent white matter related abnormalities associated with diverse molecular alterations in a mouse model of Col4a1 cerebral small vessel disease.

Gaia Brezzo[1,2] *, Alexandra Pokhilko[3]*, Jon Moss[4,5], Juraj Koudelka[1,5], Maurits A. Jansen[6] , Ross Lennen[6], Gerry Thompson[7], Sofia Marina Konstantinidou[1], Joyce Yau [6], Erin Boland[2], Anna Williams[4,5], Stuart M Allan[8,9], Alessandra Granata[10], Sanjay Sinha[11], Tao Wang[9,12], Hugh S Markus[10], Roman Fischer[13,14], M. Zameel Cader[3] , Tom Van Agtmael[2] , Karen Horsburgh[1]

* These authors contributed equally to this work

[1]Centre for Discovery Brain Sciences, University of Edinburgh, Edinburgh, UK

[2] School of Cardiovascular and Metabolic Health, University of Glasgow, University Avenue, Glasgow, G12 8QQ

[3]Translational Molecular Neuroscience Group, Weatherall Institute of Molecular Medicine, Nuffield Department of Clinical Neurosciences, University of Oxford, Oxford, OX3 9DS, United Kingdom.

[4]Centre for Regenerative Medicine, Institute for Regeneration and Repair, The University of Edinburgh, Edinburgh EH16 4UU, UK

[5] UK Dementia Research Institute, University of Edinburgh, Edinburgh, UK

[6]Centre for Cardiovascular Science, University of Edinburgh, Edinburgh, UK

[7] Centre for Clinical Brain Sciences, University of Edinburgh, Edinburgh, UK

[8] Division of Neuroscience, School of Biological Sciences, Faculty of Biology, Medicine and Health, The University of Manchester, Manchester, M13 9PT

[9]Geoffrey Jefferson Brain Research Centre, Manchester Academic Health Science Centre, Northern Care Alliance NHS Foundation Trust, University of Manchester, Manchester, UK

[10]Stroke Research Group, Department of Clinical Neurosciences Department, University of , Cambridge, Cambridge, UK

[11]Cambridge Stem Cell Institute, Jeffrey Cheah Biomedical Centre, Puddicombe Way, Cambridge CB2 0AW

[12] Division of Evolution, Infection and Genomics, School of Biological Sciences, Faculty of Biology, Medicine and Health, The University of Manchester, Manchester M13 9PT

[13]Discovery Proteomics Facility, Target Discovery Institute, Nuffield Department of Medicine, University of Oxford, Oxford, OX3 7FZ, United Kingdom.

[14] Chinese Academy of Medical Sciences Oxford Institute, Nuffield Department of Medicine, University of Oxford, Oxford, UK.

*Correspondence and request for materials should be addressed to K.H. (Chancellor's Building, 49 Little France Crescent, Edinburgh, EH16 4SB, UK. Email: karen.horsburgh@ed.ac.uk)

Abstract

White matter abnormalities are a central feature of cerebral small vessel disease (cSVD) and underpin cognitive impairment and dementia but their mechanistic link remains poorly understood. To provide insight we studied mice (*Col4a1*$^{+/Svc}$) with a mutation in the gene *Col4a1* as an established model of cSVD due to collagen IV mutations. Since collagen IV is a key component of the basement membrane, a specialised extracellular matrix structure (ECM), we hypothesised that the *Col4a1* mutation would disrupt the ECM and cause white matter abnormalities. Microstructural alterations in white matter were assessed using Magnetic Resonance diffusion tensor imaging (MR-DTI) in parallel with pathology and ultrastructural investigations of white matter. We determined that myelinating oligodendrocyte pools were reduced in parallel with prominent alterations in myelinated axons and white matter structural integrity in *Col4a1*$^{+/Svc}$ mice. Proteomic analysis of white matter revealed a significant number (n=176) of differentially expressed proteins in *Col4a1*$^{+/Svc}$ compared to controls. In particular pathways relating to the ECM and the endoplasmic reticulum (ER), including ER stress, were affected. We exploited this in a pre-clinical intervention study using the FDA-approved chemical chaperone 4-phenylbutyrate (PBA) to promote protein trafficking and reduce ER stress. PBA treatment in *Col4a1*$^{+/Svc}$ mice conferred protection against white matter defects (increasing myelinating oligodendrocytes and improving axon-glial integrity) compared to untreated *Col4a1*$^{+/Svc}$ mice. These data provide novel insight into the diversity of pathomolecular mechanisms of white matter abnormalities in cSVD and identify a modifiable pathway as a putative therapeutic target for cSVD.

Keywords:

Cerebral small vessel disease, Col4a1, white matter, proteomics, ER stress, basement membrane

Background

Cerebral small vessel disease (cSVD), a disorder of the microvasculature, is a major cause of stroke, intracerebral haemorrhage (ICH), vascular cognitive impairment and dementia [1-3]. cSVD manifests on Magnetic Resonance Imaging (MRI) as T2-white matter hyperintensities (WMH), lacunar infarcts, and cerebral microbleeds [1, 4]. These features are shared in sporadic and familial (e.g. caused by *NOTCH3; HTRA1 and COL4A1/A2* mutations) forms of cSVD. WMH that are a core feature of cSVD become increasingly common in the general population with age and predict future stroke and dementia risk [5]. The pathogenic mechanisms underlying small vessel damage and resulting in white matter injury remain debated, but evidence supports endothelial cell dysfunction, compromised blood brain barrier integrity, perfusion alterations and microvascular inflammation as key instigators [6]. Most cases of cSVD are sporadic and associated with cardiovascular risk factors particularly hypertension, although genetic predisposition also appears to be important [7]. Monogenic disorders can also cause cSVD and although rarer these are providing important insights into disease pathogenesis, with shared mechanisms between sporadic and monogenic disease being identified, particularly involving disruption of the neuro-glial-vascular unit and extracellular matrix (ECM) [8].

One monogenic familial form of cSVD is caused by mutations in the genes *COL4A1 and COL4A2,* as part of COL4A1 syndrome (also referred to as Gould Syndrome) [9]. *COL4A1/A2* encode the protein collagen IV (COL4), an important component of basement membranes (BM), a specialised ECM structure [10]. cSVD due to COL4A1/2 is characterised by typical clinical and neuroimaging features of lacunar stroke and WMH, as well as intracerebral haemorrhage (ICH) and cerebral microbleeds on MRI. Although the familial syndrome is rare, its impact on cSVD in the population may be much greater. Typical familial mutations are

much more common than expected in the general population, at about 1 per 1000, and are associated with stroke risk [2], while common non-coding polymorphic variants in *COL4A1/COL4A2* are risk factors for lacunar stroke [7], ICH [11] and WMH [12]. Thus, studies of COL4A1/2 syndrome can provide mechanistic insights into both sporadic and familial forms of SVD. Importantly however, pathomechanisms leading to white matter damage remain poorly understood and under-characterised.

There are no studies that have probed mechanistic links between COL4 and cerebral white matter abnormalities with most focussing on ICH mechanisms [13, 14] [10] [15] [16]. Given the role of COL4 as a key BM component we hypothesised that ECM defects culminate in white matter abnormalities. To address this we studied an established mouse model of SVD in *Col4a1* mutant mice (*Col4a1*$^{+/Svc}$) that harbours a glycine to aspartic acid mutation, representative of the majority of mutations found in COL4A1/2 Syndrome patients [15] [17]. Using neuroimaging, pathology and ultrastructure investigations we establish that *Col4a1* mutations cause prominent white matter alterations including reduced myelination associated with loss of myelinating oligodendrocytes. Mechanistic proteomic investigations highlighted diverse protein alterations in the white matter with the endoplasmic reticulum (ER) being a key cellular compartment that is changed. Furthermore, targeting ER stress pharmacologically conferred modest protection against white matter defects in COL4A1 disease.

Methods

Animals and PBA drug treatment

All animal experiments were conducted in accordance with the Animal (Scientific Procedures) Act 1986 and local ethical approval at the University of Edinburgh and University of Glasgow and were performed under personal and project licences granted by the Home Office. *Col4a1*$^{+/Svc}$ mice harbour a glycine to aspartate point mutation (GD1064D) in exon 37 resulting

in impaired collagen triple helix formation and stability [17]. *Col4a1*$^{+/Svc}$ on a C57BL/6J background were bred with wild type C57BL/6J mice to produce heterozygous *Col4a1*$^{+/Svc}$ and wild-type (WT) littermates. WT and *Col4a1*$^{+/Svc}$ mice were group housed on a 12-hour light/dark cycle with *ad libitum* access to food and water. Male and female mice were randomly allocated to experimental groups for studies: longitudinal MRI at 3m and 8m (*n*=8 WT, *n*=8 *Col4a1*$^{+/Svc}$), pathology at 3m (*n*=6 WT, *n*=6 *Col4a1*$^{+/Svc}$); biochemical/proteomic at 3-4m (*n*=7 WT, *n*=7 *Col4a1*$^{+/Svc}$) and electron microscopy investigations at 3-4m (*n*=3 WT, *n*=3 *Col4a1*$^{+/Svc}$). Additional cohorts were used for behavioural analysis at 8m old for nesting behaviour (*n*=6 WT, *n*=6 *Col4a1*$^{+/Svc}$) and Y-maze tasks (*n*=5 WT, *n*=6 *Col4a1*$^{+/Svc}$). The effects of long-term treatment of mice with PBA (*n*=6 WT, *n*=8 *Col4a1*$^{+/Svc}$) or vehicle (*n*=6 WT, *n*=7 *Col4a1*$^{+/Svc}$) were studied. 4-phenylbutyrate (PBA) (1 g/kg/day) [13] was administered orally via drinking water to animals from conception (by treating pregnant dams) to the end of the experiment. Animals were randomly allocated to treatment/no-treatment group before genotyping and development of overt phenotypes. Experimenters were blind to genotype status and drug treatment throughout data collection and analysis.

Brain imaging of white matter and blood flow

WT and *Col4a1*$^{+/Svc}$ mice (n=8/genotype) underwent longitudinal imaging at 3m and 8m, to assess structural (T2-weighted), white matter microstructure (diffusion tensor imaging (DTI) and cerebral blood flow (arterial spin labelling, ASL) changes as described in the supplementary methods. Experimental animals were anesthetized under 5% isoflurane in oxygen for induction then placed in an MRI compatible holder (Rapid Biomedical, Wurzburg, Germany). Isoflurane was maintained at approximately 1.5% in oxygen during scanning. Rectal temperature and respiration were monitored and controlled throughout to ensure normal physiological parameters. Structural T2-weighted and DTI MRI data were collected using a 7

T horizontal bore Biospec AVANCE preclinical imaging system with a 86 mm quadrature volume coil and a two-channel phased-array mouse brain coil. ASL was performed using a Look-Locker FAIR single gradient echo (LLFAIRGE) sequence. DTI Fractional anisotropy (FA) maps were generated in Matlab. ASL maps were generated using the Bruker software (Paravision 360). For FA and ASL measures slices corresponding to 0.14mm – -0.66mm from Bregma and -1.82mm – -2.62mm from Bregma were processed in ImageJ for region of interest analysis. At the end of imaging at 8m of age brains were processed for pathological investigations (below).

Immunohistochemical and ultrastructural investigation of white matter abnormalities

In addition to studies at 8m of age (as described above), an additional cohort of WT and *Col4a1*$^{+/Svc}$ mice (*n*=6/group) were sacrificed at 3m of age to study early pathological alterations in white matter. These mice were sacrificed under deep anaesthesia by transcardiac perfusion. PBA treated or vehicle treated mice brains were collected without saline perfusion which limited the white matter analysis that could be undertaken. Brains were post-fixed in 4% paraformaldehyde (PFA) for 24 h and embedded in paraffin wax. 6 µm thick coronal tissue sections were collected at corresponding MRI level coordinates (0.14mm and -1.82mm from Bregma). Tissue was sectioned using a rotary microtome (Leica Biosystems, Germany). Sections were used for immunostaining using standard procedures.

Briefly, sections were deparaffinised, blocked with 10% normal serum and 0.5% bovine albumin serum for 1 h at room temperature before overnight primary antibody incubation at 4 °C. Following primary incubation, sections were incubated with biotinylated secondary antibodies for 1 h at room temperature and either amplified with Vector ABC Elite Kit (Vector Labs, UK), before visualisation with 3,3′ diaminobenzidine tetrahydrochloride (DAB, Vector Labs, UK) or incubated with streptavidin (Invitrogen, UK). Myelin related abnormalities were

assessed using SMI94 (BioLegend, 836504 1:15000) and MAG (Abcam, ab89780 1:10000) immunolabelling. CC1 (Merck, OP80 1:20) immunolabelling was used as a marker of mature oligodendrocytes. Double labelling of PDGRFα (R&D, AF1062 1:200) and Ki67 (Abcam, ab16667 1:100) was carried out to assess proliferation of oligodendrocyte precursor cells (OPC). CD31 (R&D, AF3628 1:100) immunostaining was carried out to assess endothelial cell density.

A cohort of WT and *Col4a1*$^{+/Svc}$ mice (*n*=3/group) were sacrificed at 3 m of age to study early ultrastructural alterations in white matter using transmission electron microscopy (EM). Mice were transcardially perfused with saline then fixative (4% paraformaldehyde, w/v, Sigma; 0.5% glutaraldehyde, v/v; Electron Microscopy Sciences, EMS; in 0.1 M phosphate buffer, PB, Sigma), and their brains removed and post-fixed in the same fixative overnight. Brains were vibratome-sectioned coronally, at a thickness of 50 µm, post-fixed with 1% osmium tetroxide (v/v in 0.1 M PB, EMS) and dehydrated in an ascending series of ethanol dilutions (50%, 70%, 95% and 100%; Sigma) then acetone (EMS). Sections were then lifted into resin (Durcupan ACM, Fluka, Sigma), left overnight at room temperature, placed on greased microscope slides, coverslipped, and the resin cured at 65°C for 3 days. Regions of interest containing corpus callosum were cut from the slides, mounted on plastic blocks (Ted Pella) and ultrathin sectioned (70 nm thick) for electron microscopy. Ultrathin sections were collected on to meshed copper grids, contrasted with uranyl acetate and lead citrate (EMS), and imaged with a JEOL transmission electron microscope (TEM-1400 plus). EM analysis was analysed as previously published [18]. Briefly, measures of axonal diameter, myelin thickness and inner tongue thickness were calculated from measured area based on the assumption of circularity: diameter = $2 \times \sqrt{(\text{area}/\pi)}$. 100 axons per animal were analysed using Fiji/Image J (Fiji.sc). Inner tongue thickness was calculated by subtracting the axonal diameter from the diameter of the innermost compact layer. G-ratios were calculated by dividing axonal diameter by axon, inner tongue and myelin area. Percentage of myelinated axons was calculated by dividing total

number of axons by number of myelinated axons. Further qualitative analysis of abnormal phenotypes was carried out by counting axons with unfolding or unravelling of myelin and expressed as a percentage by dividing the total number of axons by total number of unfolding/unravelling axons.

Behavioural assessments

Nesting behaviour

As a measure of executive and cognitive function a nesting behaviour task was carried out on WT and *Col4a1*$^{+/Svc}$ mice (n=6/genotype). One day prior to testing mice were singularly housed to assess individual nest building. In each cage WT and *Col4a1*$^{+/Svc}$ mice received one Nestlet (composed of a pressed 2x2 inch square cotton material weighing 3g) one hour before the dark cycle. The following morning each individual nest was assessed on (1) appearance (Nestlet score), (2) height of the nest (in cm) and (3) percentage of shredded Nestlet. Scoring followed previously published criteria [19] and comparisons made between WT and *Col4a1*$^{+/Svc}$ mice.

Y-maze

Spatial working memory and spatial recognition memory were tested in a Y-maze with extra-maze visual cues to aid navigation [20]. In brief, the Y-maze apparatus consisted of three identical enclosed arms (50cm long x 11cm wide x 10cm high) made of black acrylic. The arms were mounted in the shape of a Y, set at an angle of 120° from each other, with visual cues were placed at the end of each arm. For spatial working memory (spontaneous alternation) mice were placed in the centre of the Y-maze and allowed to explore all three arms for 5 min. The number of arm entries and the sequence of arms entered were recorded. The percentage alternation was calculated as number of alternations (entries into three different arms

consecutively) divided by the total possible alternations (i.e. number of arms entered minus 2) and multiplied by 100. The number of errors the mice made were calculated as a re-entry to an arm just visited. The distance covered was also measured as an indirect measure of mobility. For spatial recognition memory, mice were placed into one of the arms of the maze (start arm) and allowed to explore the maze for 5 min with the entrance of one arm blocked off (training trial). After a 1 min -trial interval (ITI), mice were returned to the start arm of the maze for the test phase with all three arms available for exploration (for a duration of 2 min) including the novel (previously unvisited) arm. Spatial memory retention was measured as time spent in the novel arm calculated as a percentage of the total time spent in all three arms. Values were compared with the chance level for time exploring the three arms (33%).

Biochemical and proteomic investigation of white matter enriched samples

Tissue processing

WT and *Col4a1*$^{+/Svc}$ mice (n=7/genotype) were used to generate white matter enriched homogenates for biochemical and proteomic investigations. Mice were sacrificed under deep anaesthesia by transcardiac perfusion with PBS, whole brains were cut in the sagittal plane in three 2 cm slices and the corpus callosum was carefully dissected from adjacent grey matter. Following isolation of the corpus callosum, samples were homogenised in 1:10 (vol:vol) ice-cold RIPA buffer using a glass hand-held loose fit dounce homogenisers with 25 strokes. Samples were sonicated for 5 s and maintained in constant agitation for 2 h at 4 °C. Finally, samples were centrifuged at 5000g for 2 min and the supernatant collected.

Proteomics

Up to 20 µg of white matter homogenate were prepared for LC-MS analysis using a 96-well S-Trap plate (Protifi LCC) following the protocol as provided by the manufacturer. Briefly,

samples were reduced with 5 µl 200 mM DTT and alkylated with 20 µl 200 mM IAM for 30 min each, acidified with 12% phosphoric acid 10:1 (v/v) sample to acid, transferred into the S-Trap well and precipitated with 7 parts 90% methanol in 100 mM TEAB to 1 part sample (v/v). Samples were washed 3x by spinning the S-trap plate at 1500xg for 30 s and the last step for 1 min, each time with fresh 90% methanol in 100 mM TEAB. The sample was resuspended in 50 µL 50 mM TEAB and digested with 0.8 µg trypsin (Promega) over night at 37°C in an incubator. Peptides were eluted from the S-Trap by spinning for 1 min at 1500xg with 80 µL 50 mM ammonium bicarbonate, 80 µL 0.1% FA and finally 80 µL 50% ACN, 0.1% FA. The eluates were dried down in a vacuum centrifuge and resuspended in loading buffer (2% ACN, 0.1% TFA) prior to high pH prefractionation and mass spectrometry acquisition.

High pH prefractionation on Agilent Bravo Assaymap

RP-S cartridges were primed with 100 µL ACN at 300 µL/min, equilibrated with 50 µL loading buffer (2% ACN, 0.1% TFA) at 10 µL/min followed by loading 120 µL sample at 5 µL/min. the cartridge cup was washed with 50 µL and an internal cartridge wash was performed with 25 µL loading buffer at 5 µL/min. Eight subsequent elution steps were done with buffer A (Water, pH 10) and buffer B (90% ACN, pH 10) at the following percentages of buffer B: 5%, 10%, 12.5%, 15%, 20%, 22.5%, 25% and 50%. The eluates of the following steps were directly concatenated 1+5, 2+6, 3+7 and 4+8. Fractions were dried down in a vacuum centrifuge and resuspended in loading buffer.

LC-MS/MS data acquisition

Peptides were analysed by LC-MS/MS as described [21]. Briefly, peptides were separated on a nEASY column (PepMAP C18, 75 µm x 500mm, 2 µm particle, Thermo) using a linear gradient of 2%-35% Acetonitrile in 5% DMSO/0.1% Formic acid at 250nl/min. MS data was acquired on a Q-Exactive mass spectrometer in DDA mode. MS1 resolution was set to 70,000

with an AGC target of 3E6. The top 15 most abundant precursors were selected for MS/MS with a resolution of 17,500, AGC target of 6E3 and an isolation window of 1.6 m/z. Fragments were generated with a normalized collision energy of 28% and selected precursors were excluded for 27 seconds.

Data analysis and protein identification and quantification

The proteomics analysis was based on protein identifications by MaxQuant. The raw data files were searched against either the reviewed Uniprot homo sapiens databased (retrieved 20180131) or mus musculus (retrieved 20190304) using MaxQuant [22] version 1.6.10.43 and its built-in contaminant database using tryptic specificity and allowing two missed cleavages. The results were filtered to a 1% FDR.

More than 2000 proteins were identified in each mouse white matter sample with at least two unique peptides, except one outlier WT sample, which had only 411 proteins and therefore was removed from the analysis. Differential protein analysis was done using 2595 proteins identified in both groups (WT and *Col4a1*$^{+/Svc}$) in at least three biological replicates. Intensity values were normalized (divided) to median values in each sample to correct for between-sample differences, and missing values were replaced by median intensities for each protein in both groups [23, 24]. The analysis of the differences in protein levels between the groups was done with limma package in R using empirical Bayes method for two group comparison with the t-test of the eb.fit function [25]. The results were visualized on volcano plots with significance level $p \leq 0.05$ and fold changes ≥ 1.5. All proteins from the differential analysis were combined in a single Excel sheet with all relevant information, including the annotation and location scores from String database [26].

The pathways and protein-protein interactions (PPI) network analysis were done using all the proteins identified during the differential analysis, including proteins exclusively present in only one group in ≥ three replicates, and present at zero levels in all samples of another group.

The pathway network analysis was done using ClueGO plug-in [27] in Cytoscape [28] with KEGG and GO BP (Biological processes) databases. Only significantly enriched pathways were retained on the network (FDR<=0.05). The PPI network was constructed using StringApp in Cytoscape, retaining only high confidence interactions were retained, and proteins disconnected from the main network were omitted (except those present in the significantly enriched pathways from the ClueGO analysis). The location scores predicted by String database were used to colour the proteins according to their potential location based on the following prioritisation criteria: 1) proteins with high ER, endosome or golgi location scores (between 3 and 5=max) were assigned into group 1; 2) proteins with high mitochondria location score, but low score for the group 1 were assigned to the group 2; 3) proteins with high cytosol or cytoskeleton location scores, which were not present in groups 1 and 2 were assigned to the group 3; 4) proteins with high extracellular score, but low for the above groups were assigned to the group 4. Similarly, groups 5 and 6 consisted of the proteins with high plasma membrane or nuclear scores respectively, which were not present in the above groups.

Statistical analysis

MRI data (FA, ASL) were analysed by two-way mixed measures ANOVA with age and genotype as main factors with post-hoc Bonferroni. Immunohistochemistry/immunofluorescent and behavioural data were analysed by two-way ANOVA with post-hoc Tukey or Bonferroni. For MAG grading this was analysed using Kruskal-Wallis with post hoc Dunn's test. EM data was analysed with t-test. All statistical analysis was performed using Graphpad Prism (v5, Graphpad Software Inc.) or SPSS (v23, IBM Corporation). $p<0.05$ was considered to be a significant effect.

Results

Col4a1$^{+/Svc}$ mice show widespread white matter alterations

To examine the effect of the *Col4a1* GD1064D mutation on white matter health, longitudinal fractional anisotropy (FA) measures were taken from *Col4a1$^{+/Svc}$ (n*=8) and WT animals (*n*=8) at 3 and 8 m of age. White matter changes were assessed at two anatomical levels of the corpus callosum (Bregma 0.14 mm and Bregma -1.82 mm) and the internal capsule (Bregma -1.82 mm) (Figure 1A). Mixed measures two-way ANOVA results indicate overall differences in FA between genotype in corpus callosum at Bregma level 0.14 mm ($F(1,14)=8.14$, $p=.013$), at Bregma -1.82 mm ($F(1,14)=13.3$, $p=.003$) and internal capsule ($F(1,14)=20.85$, $p<.001$). A significant age effect was also identified in the corpus callosum (Bregma 0.14 mm) $F(1,14)=46,33$, $p<.001$) as well as significant interactions effects (Age*Genotype) in corpus callosum (Bregma -1.82mm) (($F(1,14)=5.18$, $p=.039$) and internal capsule $F(1,14)=7.51$, $p=.016$) (Supplementary Table1). *Post hoc* tests (Figure 1B) reveal significant decreases in FA in *Col4a1$^{+/Svc}$* animals compared to WT littermates across the examined white matter regions, as well as age associated changes in the corpus callosum (Bregma level 0.14 mm).

To further define if the white matter alterations observed on MR-DTI were due to demyelination and/or axonal pathology, we performed a series of immunohistochemical investigations. Immunostaining for MAG, present at the axon-glia interface, revealed widespread accumulation of MAG^{+} myelin debris, across caudal (Bregma 0.14 mm) and rostral (Bregma -1.82 mm) corpus callosum and internal capsule in both age groups (Figure 1C,D; Supplementary Figure 1). Immunostaining for SMI94 (Figure 1E,F), a myelin basic protein marker, reveals demyelination of caudal (Bregma 0.14 mm) corpus callosum in *Col4a1$^{+/Svc}$* mice compared to WT. Two-way ANOVA analysis reveal a significant effect of genotype ($F(1,24) = 10.74$, $p=0.003$) and a significant effect of age ($F(1,24) = 7.318$, $p=0.012$), but no genotype and age interaction ($F(1, 24) = 0.631$, $p=0.435$). Assessment of callosal thickness

across WT and *Col4a1*$^{+/Svc}$ mice reveals white matter atrophy in *Col4a1*$^{+/Svc}$ mice, with a significant effect of genotype (F (1,24) = 10.74, p<.001) but no significant effect of age (F(1,24) = 4.06, p=0.055), or interaction (F(1, 24) = 0.16, p=0.902) (Figure 1G). Therefore, the MR-DTI changes can be explained at least in part by myelin loss.

Early ultrastructural white matter abnormalities in Col4a1$^{+/Svc}$ mice

Ultrastructural investigations were undertaken to provide further detail on the changes within the corpus callosum of WT and *Col4a1*$^{+/Svc}$ mice (n=3/genotype) (Figure 2A). Quantification of myelinated axons on micrographs (Figure 2B) indicated there was a significant reduction in both axonal diameter (t(4)=3.16, p=0.034) and myelin thickness (t(4)=3.7, p=0.021) in *Col4a1*$^{+/Svc}$ mice compared to WT littermates (Figure 2B). However, there was no change in the inner tongue thickness (t(4)=1.44, p=0.22) or G-ratio of myelinated axons (t(4)=0.72, p=0.51). Overall, *Col4a1*$^{+/Svc}$ mice had 40% fewer myelinated axons compared to WT animals (t(4)=5.47, p=0.005) (Figure 2C). *Col4a1*$^{+Svc}$ animals also showed significantly more abnormal phenotypes (see Figure 2D) including blebbing, outfoldings of myelin or unravelling of myelin sheaths compared to WT mice (t(4)=7.0, p=0.002). These results support our initial MRI and histopathological observations of both myelin and axonal pathology in *Col4a1*$^{+/Svc}$ mice.

Mature myelinating oligodendrocytes are reduced in Col4a1$^{+/Svc}$ mice

To shed light on underlying mechanisms behind these white matter changes, we first focused on mature myelinating oligodendrocytes (OLs), which are critical for the production, maintenance and regulation of axon myelination, enabling efficient neuronal communication, therefore maintaining cognitive function. Furthermore, as myelin is continuously remodelled in the CNS, turnover of mature OLs, from oligodendrocyte precursor cells (OPCs) is vital.

Given the importance of both mature OLs and OPCs to maintain efficient myelination, we next investigated OLs and OPC integrity in *Col4a1*$^{+/Svc}$ mice.

We firstly determined the numbers of mature myelinating OLs, stained with CC1, and found reduced numbers of mature OLs in Col4a1$^{+/Svc}$ mice compared to WT. Two way ANOVA analysis reveal a significant effect of genotype ($F(1,24)=15.05$ $p<0.001$) and age ($F(1,24)=4.896$, $p=0.037$) and no interaction ($F(1,24)=0.86$, $p=0.772$) (Figure 3A-B). Reduced numbers of mature OLs could be a result of impaired proliferation, impaired differentiation and/or apoptosis of mature OLs. To unravel underlying mechanisms, we next investigated the numbers and proliferation capacity of OPCs. We found a modest reduction in numbers of OPCs (stained by PDGFRα) in *Col4a1*$^{+/Svc}$ mice compared to WT. There was a significant effect of genotype ($F(1,24)=5.205$, $p=0.032$), but no significant effect of age ($F(1,24)=2.847$, $p=0.104$) or interaction ($F(1,24)=1.986$, $p=0.172$) (Figure 3C-D). Interestingly, by using Ki67 as a proliferative marker to quantify numbers of proliferating OPC numbers (PDGFRa+Ki67+ cells), we observed an increased proliferation at 3 m of age in *Col4a1*$^{+/Svc}$ mice (Figure 3C,E). Two-way ANOVA results indicate significant effects of genotype ($F(1,24)=5.505$, $p=0.028$), age ($F(1,24)=5.29$, $p=.030$) and genotype*age interaction ($F(1,24)=8.018$, $p=0.009$). This indicates proliferation capacity is not impaired in OPCs and does not account for the decreased numbers of mature OLs in *Col4a1*$^{+/Svc}$ mice. On the contrary, at least in young *Col4a1*$^{+/Svc}$ animals, OPC proliferation is increased, potentially to help remedy the loss of mature OLs caused by the *Col4a1* mutation.

Endothelial cell density and CBF alterations in white matter in Col4a1$^{+/Svc}$ mice

OPCs require the cerebral endothelium and adjacent BM, as a physical substrate and as trophic support for their proliferation, migration, differentiation and survival [29]. Endothelial cell (EC) function and density can be reduced in cSVD and thus we wanted to determine if these

are altered by the *Col4a1* mutation which may help explain the observed alterations in OPCs and OLs. EC density, identified as CD31+ve immunostaining, was measured in the corpus callosum (Bregma level 0.14 mm) corresponding to white matter changes detected previously. We observed increased CD31 area coverage in *Col4*$^{+/Svc}$ animals compared to WT littermates. Two-way ANOVA revealed a significant effect of genotype ($F(1,24)=26.42$, $p<0.001$) and age ($F(1,24)=4.93$ $p=0.036$). No significant interaction was observed ($F(1,24)=0.786$, $p=0.384$).

Interestingly, in support of increased EC density, we also found increased cerebral perfusion, as measured by ASL in the same region of corpus callosum (Bregma 0.14 mm) in *Col4a1*$^{+/Svc}$ compared to WT mice. Two-way mixed measures ANOVA results indicate overall differences between genotype ($F(1,14)=20.44$, $p<0.001$), age ($F(1,14)$-7.46, $p=0.016$) and an age*genotype interaction ($F(1,14)$-10.82, $p=0.005$). *Post hoc* tests (Figure 4D) reveal significant increases in CBF in *Col4a1*$^{+/Svc}$ animals compared to WT littermates at 3 m of age ($p=0.001$) and a reduction in CBF comparing *Col4*$^{+/Svc}$ animals at 3 and 8 m of age ($p=0.003$). Increased cerebral perfusion was also detected in other white matter regions (including internal capsule) in *Col4a1*$^{+/Svc}$ compared to WT mice (see Supplementary Table 2). Thus, white matter alterations in *Col4a1*$^{+/Svc}$ mice cannot be attributed to reduced perfusion via reduced EC density.

Col4a1$^{+/Svc}$ *mice display impairment of cognition and executive function.*

Given the profound alterations in white matter integrity in *Col4a1*$^{+/Svc}$ *mice*, we next investigated the impact of these changes on behavioural and cognitive functions using a battery of tests at 8mo of age (see Supplementary Figure 2). Behaviour was firstly assessed with a nesting task (Supplementary Figure 2A), which we have previously showed to be a sensitive marker for executive function [30]. Nest appearance was overall significantly lower for *Col4a1*$^{+/Svc}$ mice compared to WT littermates ($p=0.012$) (Supplementary Figure 2B).

Following this, WT and *Col4a1*$^{+/svc}$ mice (n=5/6) underwent further behavioural testing in Y-maze to assess spatial working and spatial recognition memories (Supplementary Figure 2C). Alternation tasks are commonly used to evaluate exploratory behaviour and working memory [31]. Upon being placed in the Y-maze and in the pursuit of novelty, mice adopt a pattern of exploration whereby each of the three arms are entered consecutively without a repeat entry to an arm just visited (Supplementary Figure 2C). There was no significant difference in the percentage of spontaneous alternation of arm entries between WT and *Col4a1*$^{+/Svc}$ mice (p=0.36) (Supplementary Figure 2D). Further analysis of the percentage of errors (as an index of short-term working memory) revealed a non-significant (p=0.061) trend towards more errors in the *Col4a1*$^{+/Svc}$ mice (Supplementary Figure 2E). To check if there were differences in locomotor activity, distance travelled in the Y-maze was measured. *Col4a1*$^{+/Svc}$ mice travelled a similar distance to WT, indicating intact locomotor activity (p=0.126) (Supplementary Figure 2F).

To assess short-term spatial recognition memory, which is dependent on the hippocampus, a two-trial (acquisition and retention) Y-maze test with a 1min ITI was used (Supplementary Figure 2C). In the acquisition phase with one arm of the Y-maze closed, mice are placed in the 'start' arm and allowed to explore this arm and the 'other' arm and the % time spent in these two arms calculated. There was no significant difference for the %time spent in start (p=0.942) and other (p=0.991) arms between the WT and *Col4a1*$^{+/Svc}$ mice. However, following 1min ITI with all three arms of the Y-maze available for exploration, *Col4a1*$^{+/Svc}$ mice spent a significantly lower percentage of time exploring the novel (previously unvisited) arm compared to WT mice (p=0.004) ((Supplementary Figure 2G). Collectively, these studies indicate that the *Col4a1* mutation affects behavioural measures including cognitive and executive brain function.

Proteomic investigation of white matter alterations in Col4a1$^{+/Svc}$ *mice highlights ER stress and ECM defects.*

To gain insight into the underlying molecular changes that could explain the white matter abnormalities in *Col4a1*$^{+/Svc}$ mice, we combined mass spectrometry with off-line high-pH reversed-phase fractionation to increase proteome coverage and power to detect protein differences between WT (n-=6) and *Col4a1*$^{+/Svc}$ mice (n=7). More than 2000 proteins were identified in each sample. Differential analysis revealed that 142 out of 2579 proteins, which were identified in at least three biological replicates in each group, were present at significantly different levels between WT and *Col4a1*$^{+/Svc}$ animals (p value ≤ 0.05, fold change ≥ 1.5; Fig. 5A). In addition, 34 proteins were identified exclusively in *Col4a1*$^{+/Svc}$ mice resulting in a total of 176 proteins (Supplementary Table 3) being differentially expressed (Fig. 5A).

To further explore the biological function of these differentially expressed proteins, we performed pathway analysis with ClueGO plug-in in Cytoscape, using KEGG and GO BP databases. ECM and axon-related terms were significantly represented amongst the pathways that were differentially regulated between WT and *Col4a1*$^{+/Svc}$ mice (Fig. 5B, Supplementary Table 3), in agreement with experimental observations. In addition, epithelial cell differentiation, endocytosis, GTPases activity and ionic/osmotic changes were significantly represented, suggesting the involvement of these processes in the observed pathological changes in the Col4a1$^{+/Svc}$ mice. To further explore the potential location and inter-relationships between the differentially expressed proteins, we constructed a String PPI network in cytoscape. This showed that many of the proteins were located to ER and mitochondria, as well as to the extracellular and plasma membrane (Fig. 5C). Furthermore, many of the differentially expressed proteins were related to the ER/mitochondrial stress responses (e.g., Ubxn1, Tigar, Dnm1l, Slc6a9, Supplementary Table 3), which we previously showed in *Col4a1*$^{+/Svc}$ mice [32] [13].

PBA treatment modestly ameliorates white matter abnormalities in *Col4a1*$^{+/Svc}$ ***mice***

Following on from the findings that the ER was a key cellular compartment altered with the *Col4a1* mutation and that many differentially expressed proteins were related to ER stress proteins; we next explored whether targeting protein folding in the ER could exert white matter protection. Mice were treated orally with the FDA-approved compound, PBA which promotes protein trafficking and reduces ER stress, from conception (WT n=7, *Col4a1*$^{+/Svc}$, n=8) and compared to cohorts of untreated WT (n=6), and *Col4a1*$^{+/Svc}$ (n=7) mice.

We firstly undertook MAG immunostaining to assess axon-glial integrity (Figure 6A), which we had previously shown to be sensitive to white matter abnormalities in *Col4a1*$^{+/Svc}$ mice (Figure 1). Evidence of breakdown in axon-glial integrity was detected as an accumulation of myelin debris and graded [33] . Notably, untreated *Col4a1*$^{+/Svc}$ mice displayed a significantly greater extent of axon-glial breakdown compared to PBA treated *Col4a1*$^{+/Svc}$ mice (p=0.034) providing evidence that improving protein folding is beneficial in the presence of the *Col4a1* mutation. Unexpectedly, more MAG+ debris was detected in PBA treated compared to untreated WT mice (p=0.045) i.e. in the healthy mouse brain.

The effects of PBA on the number of myelinating oligodendrocytes (CC1+ cells) was also measured (Figure 6C). Two-way ANOVA demonstrated no significant effect of genotype ($F(1,24)=0.02748$; $p=0.8698$), or treatment ($F(1,24)=1.259$; $p=0.2734$). However, an interaction effect between genotype and PBA treatment was revealed ($F(1,24)=12.68$; $p=0.0017$). Post-hoc analysis showed PBA treatment significantly increased the number of myelinating oligodendrocytes in the Col4a1$^{+/svc}$ mice compared to those that were untreated (p=0.0095) (Figure 6D). Thus, the improved axon-glial integrity in PBA treated Col4a1$^{+/svc}$ mice may be attributed to increased numbers of myelinating oligodendrocytes. These data support a beneficial effect of PBA and targeting ER stress on white matter defects in SVD due to a *Col4a1* mutation.

Discussion

White matter abnormalities are a prominent feature of familial and sporadic forms of cSVD and linked to risk of cognitive impairment and dementia. Here we established that in a well-established mouse model of SVD, due to *Col4a1* mutation, there are white matter defects with increased myelin debris and reduced number of oligodendrocytes, leading to impaired cognitive brain function. Moreover, we reveal these defects are associated with extensive changes to ER and ECM proteins. Importantly, targeting ER protein folding using the chemical chaperone PBA partially rescued these white matter defects and oligodendrocyte number, informing on a future putative treatment strategy for cSVD associated with collagen IV variants.

Collagen IV has emerged as an important factor in cSVD as not only do *COL4A1/2* mutations cause a genetic form of cSVD but rare mutations also occur in sporadic cSVD and common non-coding variants are a risk factor for sporadic SVD. $Col4a1^{+/Svc}$ mice harbour a specific glycine to aspartic acid mutation [G1064D] that maps to >85% of mutations identified in patients to date [9] and thus is a clinically relevant powerful model to study cSVD disease mechanisms. Our neuroimaging approaches, (MR-DTI), which we previously determined to be sufficiently sensitive to detect microstructural alterations in damaged white matter in the rodent brain [34] [35] showed that FA was significantly reduced in a number of white matter tracts including the corpus callosum in $Col4a1^{+/Svc}$ mice. These changes were evident at 3 m of age and sustained until 8 m of age. Notably, in the same animals, we observed extensive white matter damage including an overall loss of myelinated axons and mature myelinating oligodendrocytes consistent with atrophy of the corpus callosum in $Col4a1^{+Svc}$ mice. Ultrastructural alterations in myelinated axons were also evident in $Col4a1^{+Svc}$ mice.

A prevailing view proposes cerebral hypoperfusion as a central common mechanism underlying white matter abnormalities in cSVD. However, studies are often cross sectional in nature and CBF related mechanisms are not always investigated in relation to white matter integrity [36]. We used ASL neuroimaging to quantify regional alterations in CBF in white matter regions in the *Col4a1*$^{+Svc}$ model compared to controls and found an increase in CBF at 3 m of age which then subsided by 8 m of age, which associated with evidence of increased microvascular density and remodelling. This is contrary to previous studies in Col4a1^{+Svc} mice where there was a loss of vascular function and tone with enhanced vasodilatory capacity [37]), and so our finding may reflect early disease mechanisms that precede later suppression/reduction of CBF. In another *Col4a1*mutant mouse model, *Col4a1*$^{+/G394V}$, impaired blood flow responses to neural stimulation were also observed supporting a loss of vascular function in COL4A1 disease [38]. Although clinical studies that have investigated regional CBF alterations early in cSVD are lacking, cerebral hyperperfusion has been reported in asymptomatic APOE4 individuals with white matter disruption before the onset of dementia [39]. Consistent with defects in white matter integrity, *Col4a1*$^{+Svc}$ mice displayed behavioural and memory problems by 8m of age with impairment of short-term spatial recognition memory. In a milder Col4a1 mutant model (Col4a1$^{+/G394V}$) impaired working memory has been reported at 12m of age and attributed to vascular related defects [38]. However, given the prominent white matter alterations determined in *Col4a1*$^{+Svc}$ mice it would be important to determine if these changes are consistent across different forms of COL4 disease. Importantly, our finding of impaired short-term spatial memory in a Y-maze with extra-maze cues align with the clinical condition which show impaired spatial navigation in human SVD [40].

We gained mechanistic insight to the underlying molecular changes of the observed white matter defects by an unbiased proteomic approach. Mass spectrometry with off-line high-pH reversed-phase fractionation was used, as we previously reported this approach to be effective in increasing the proteome depth by 3-4 fold [41]. We identified 176 proteins that were

significantly different between WT and *Col4a1*$^{+Svc}$ mice, and given that collagen IV is an ECM protein, making up the vascular BM [41], it is unsurprising that many key ECM-related proteins were upregulated in the *Col4a1*$^{+Svc}$ mice (eg Lamb2, Lamc1, Nid2, Hapln2). In addition, Mia3 (ER protein involved in the secretion of collagens and especially large cargos), Serpinh1 (involved in collagen biosynthesis), as well as GTPase Rala (involved in integrin signalling associated with exocytosis) were increased in *Col4a1*$^{+Svc}$ mice. Many proteins that were altered were involved in stress responses, and these were all upregulated in *Col4a1*$^{+Svc}$ mice, including those linked to ER stress (eg Ubxn1, Slc6a9 and Capns1) or linked to hypoxia/oxidative stress (eg Tagln2, Clpp, Aqp1, Slc25a10). A number of stress-related proteins were also found to be involved in axonal growth including ubiquitin-specific protease Usp47, Stmn2 and the Rho GTPase-activating protein Arhgap23, linking ECM dysfunction and axon stability. Other upregulated proteins in *Col4a1*$^{+Svc}$ mice were related to endothelial cell functions including actin-binding protein Flna (involved in ciliogenesis and formation of adherens junctions during vascularization) and an activator of Rho and Rac GTPases, Dock5, involved in EC migration. In addition, a negative regulator of VEGF-induced angiogenesis Rock1 was downregulated in *Col4a1*$^{+Svc}$, suggesting increased EC angiogenesis supporting our finding of increased EC density and cerebral perfusion in the *Col4a1*$^{+Svc}$ mice. Other downregulated proteins in *Col4a1*$^{+Svc}$ mice included apoptotic membrane protein Dnm1l induced by oxidative stress; mitochondrial pro-apoptotic stress inducer Slc25a23 and ionic carrier Slc8a1, which is reduced by oxidative stress, suggesting activation of both apoptotic and stress-protecting mechanisms.

Treatment of *Col4a1*$^{+Svc}$ mice with PBA, a compound that promotes the trafficking of misfolded proteins and alleviates ER stress, increased OL numbers and improved white matter integrity in *Col4a1*$^{+Svc}$ mice, but was not fully restorative. These findings extend our previous investigations [13] and others [9] that showed a beneficial effect of PBA on ICH - another consequence of *Col4a1* mutations, and complements beneficial manipulation of ECM by MMP

inhibition as previously described in a iPSC human model of *COL4A1/A2* disease [42]. Our proteomic data suggest a diversity of protein alterations and pathways are damaged in white matter in *Col4a1*$^{+Svc}$ mice providing a wealth of other potential targets. Targeting protein folding as therapy has been considered in the treatment of other neurodegenerative disorders [43] and it remains to be determined whether this approach would be of benefit in treating cSVD related white matter pathology.

Availability of data and material

The mass spectrometry proteomics data have been deposited to the ProteomeXchange Consortium via the PRIDE partner repository with the dataset identifier PXD057204. The processed data are supplied as Supplementary Tables.

Acknowledgements

We would like to acknowledge the contributions of students Dan Sandler, Sara Castro Devesa, Nela Fialova, Siham Nimale, Oonagh Thin, Cameron Thomson (University of Edinburgh) who helped provide preliminary analysis of MRI, immunohistochemical and behavioural studies. The technical support provided by Steve Mitchell at the TEM facility, University of Edinburgh and Raphael Heilig at the Discovery Proteomics Facility, University of Oxford are gratefully appreciated.

Authors' contributions

K.H. directed and designed the research study. G.B. performed the neuroimaging studies with support from M.J, R.L. and G.T. G.B. J.M., A.W. were responsible for the ultrastructural studies and analysis. G.B. was responsible for the immunohistochemical studies and analysis. R.F. was responsible for LC-MS analysis. A.P. and L.H. undertook the downstream proteomic analysis. E.B performed intervention study with direction from T.V.A.. G.B., A.P., L.H., K.H. and Z.C. analyzed and interpreted the data with critical input from T.V.A.. A.N., A.G., S.S., T.W., H.S.M. and S.A.N. provided critical reading of the manuscript. K.H. wrote the manuscript with support from G.B. and A.P. and T.V.A with comments from all authors. All authors edited the manuscript and approved the final submission.

Funding

This research reported in this publication was primarily supported by a Stroke Association priority programme award in Advancing Care and Treatment of Vascular Dementia (grant reference number 16VAD_04) in partnership with the British Heart Foundation (BHF) and Alzheimer's Society (SA, ZC, AG, KH, HM, SS, TW, TVA). KH received funding support from the Alzheimer's Society (290 (AS-PG-15b-018); 228 (AS-DTC-2014-017)) and Alzheimer's Research UK (ARUK) (ARUK-PG2016B-6). TVA was funded by the Medical Research Council (MRC) (MR/R005567-1), BHF (PG/15/92/31813), and Heart Research UK (RG 2664/17/20). SS was also funded by BHF Fellowship (FS/18/46/33663) and the Cambridge BHF Centre for Research Excellence (RE/18/1/34212). SMA was funded by BHF (PG/17/86/33399) and Leducq Foundation (19CVD01). ZC received funding support from the EU/EFPIA Innovative Medicines Initiative 2 Joint Undertaking (IM2PACT grant no. 807015); from National Institute for Health Research (NIHR) Oxford Biomedical Research Centre (BRC); and from MRC (MC_PC_16034).

Declarations

Competing interests

The authors declare no competing interests.

References

1. Wardlaw, J.M., C. Smith, and M. Dichgans, *Small vessel disease: mechanisms and clinical implications.* Lancet Neurol, 2019. **18**(7): p. 684-696.
2. Cho, B.P.H., et al., *Association of Vascular Risk Factors and Genetic Factors With Penetrance of Variants Causing Monogenic Stroke.* JAMA Neurol, 2022. **79**(12): p. 1303-1311.
3. Markus, H.S. and F.E. de Leeuw, *Cerebral small vessel disease: Recent advances and future directions.* Int J Stroke, 2023. **18**(1): p. 4-14.
4. Duering, M., et al., *Neuroimaging standards for research into small vessel disease-advances since 2013.* Lancet Neurol, 2023. **22**(7): p. 602-618.
5. Debette, S., et al., *Clinical Significance of Magnetic Resonance Imaging Markers of Vascular Brain Injury: A Systematic Review and Meta-analysis.* JAMA Neurol, 2019. **76**(1): p. 81-94.
6. Horsburgh, K., et al., *Small vessels, dementia and chronic diseases - molecular mechanisms and pathophysiology.* Clin Sci (Lond), 2018. **132**(8): p. 851-868.
7. Traylor, M., et al., *Genetic basis of lacunar stroke: a pooled analysis of individual patient data and genome-wide association studies.* Lancet Neurol, 2021. **20**(5): p. 351-361.
8. Joutel, A., et al., *Perturbations of the cerebrovascular matrisome: A convergent mechanism in small vessel disease of the brain?* J Cereb Blood Flow Metab, 2016. **36**(1): p. 143-57.
9. Kuo, D.S., C. Labelle-Dumais, and D.B. Gould, *COL4A1 and COL4A2 mutations and disease: insights into pathogenic mechanisms and potential therapeutic targets.* Hum Mol Genet, 2012. **21**(R1): p. R97-110.
10. Gatseva, A., et al., *Basement membrane collagens and disease mechanisms.* Essays Biochem, 2019. **63**(3): p. 297-312.
11. Rannikmae, K., et al., *Common variation in COL4A1/COL4A2 is associated with sporadic cerebral small vessel disease.* Neurology, 2015. **84**(9): p. 918-26.
12. Persyn, E., et al., *Genome-wide association study of MRI markers of cerebral small vessel disease in 42,310 participants.* Nat Commun, 2020. **11**(1): p. 2175.
13. Jones, F.E., et al., *4-Sodium phenyl butyric acid has both efficacy and counter-indicative effects in the treatment of Col4a1 disease.* Hum Mol Genet, 2019. **28**(4): p. 628-638.
14. Chung, J., et al., *Rare Missense Functional Variants at COL4A1 and COL4A2 in Sporadic Intracerebral Hemorrhage.* Neurology, 2021. **97**(3): p. e236-e247.
15. Zagaglia, S., et al., *Neurologic phenotypes associated with COL4A1/2 mutations: Expanding the spectrum of disease.* Neurology, 2018. **91**(22): p. e2078-e2088.
16. Murray, L.S., et al., *Chemical chaperone treatment reduces intracellular accumulation of mutant collagen IV and ameliorates the cellular phenotype of a COL4A2 mutation that causes haemorrhagic stroke.* Hum Mol Genet, 2014. **23**(2): p. 283-92.
17. Van Agtmael, T., et al., *Dominant mutations of Col4a1 result in basement membrane defects which lead to anterior segment dysgenesis and glomerulopathy.* Hum Mol Genet, 2005. **14**(21): p. 3161-8.
18. Dillenburg, A., et al., *Activin receptors regulate the oligodendrocyte lineage in health and disease.* Acta Neuropathol, 2018. **135**(6): p. 887-906.
19. Deacon, R.M., *Assessing nest building in mice.* Nat Protoc, 2006. **1**(3): p. 1117-9.
20. Yau, J.L., et al., *Enhanced hippocampal long-term potentiation and spatial learning in aged 11beta-hydroxysteroid dehydrogenase type 1 knock-out mice.* J Neurosci, 2007. **27**(39): p. 10487-96.
21. Stepanova, S. and V. Kasicka, *Analysis of proteins and peptides by electromigration methods in microchips.* J Sep Sci, 2017. **40**(1): p. 228-250.
22. Cox, J., et al., *Andromeda: a peptide search engine integrated into the MaxQuant environment.* J Proteome Res, 2011. **10**(4): p. 1794-805.
23. Gromski, P.S., et al., *Influence of missing values substitutes on multivariate analysis of metabolomics data.* Metabolites, 2014. **4**(2): p. 433-52.
24. Wei, R., et al., *Missing Value Imputation Approach for Mass Spectrometry-based Metabolomics Data.* Sci Rep, 2018. **8**(1): p. 663.

25. Kammers, K., et al., *Detecting Significant Changes in Protein Abundance.* EuPA Open Proteom, 2015. **7**: p. 11-19.
26. Szklarczyk, D., et al., *STRING v11: protein-protein association networks with increased coverage, supporting functional discovery in genome-wide experimental datasets.* Nucleic Acids Res, 2019. **47**(D1): p. D607-D613.
27. Bindea, G., et al., *ClueGO: a Cytoscape plug-in to decipher functionally grouped gene ontology and pathway annotation networks.* Bioinformatics, 2009. **25**(8): p. 1091-3.
28. Shannon, P., et al., *Cytoscape: a software environment for integrated models of biomolecular interaction networks.* Genome Res, 2003. **13**(11): p. 2498-504.
29. Tsai, H.H., et al., *Oligodendrocyte precursors migrate along vasculature in the developing nervous system.* Science, 2016. **351**(6271): p. 379-84.
30. Hase, Y., et al., *Effects of environmental enrichment on white matter glial responses in a mouse model of chronic cerebral hypoperfusion.* J Neuroinflammation, 2017. **14**(1): p. 81.
31. Kraeuter, A.K., P.C. Guest, and Z. Sarnyai, *The Y-Maze for Assessment of Spatial Working and Reference Memory in Mice.* Methods Mol Biol, 2019. **1916**: p. 105-111.
32. Jones, F.E., et al., *ER stress and basement membrane defects combine to cause glomerular and tubular renal disease resulting from Col4a1 mutations in mice.* Dis Model Mech, 2016. **9**(2): p. 165-76.
33. Coltman, R., et al., *Selective white matter pathology induces a specific impairment in spatial working memory.* Neurobiol Aging, 2011. **32**(12): p. 2324 e7-12.
34. Holland, P.R., et al., *MRI is a sensitive marker of subtle white matter pathology in hypoperfused mice.* Neurobiol Aging, 2011. **32**(12): p. 2325 e1-6.
35. Holland, P.R., et al., *Gliovascular disruption and cognitive deficits in a mouse model with features of small vessel disease.* J Cereb Blood Flow Metab, 2015. **35**(6): p. 1005-14.
36. Shi, Y., et al., *Cerebral blood flow in small vessel disease: A systematic review and meta-analysis.* J Cereb Blood Flow Metab, 2016. **36**(10): p. 1653-1667.
37. Van Agtmael, T., et al., *Col4a1 mutation in mice causes defects in vascular function and low blood pressure associated with reduced red blood cell volume.* Hum Mol Genet, 2010. **19**(6): p. 1119-28.
38. Yamasaki, E., et al., *Impaired intracellular Ca(2+) signaling contributes to age-related cerebral small vessel disease in Col4a1 mutant mice.* Sci Signal, 2023. **16**(811): p. eadi3966.
39. Mak, E., et al., *Proximity to dementia onset and multi-modal neuroimaging changes: The prevent-dementia study.* Neuroimage, 2021. **229**: p. 117749.
40. Zhao, H., et al., *Spatial Navigation Is Impaired in Elderly Patients With Cerebral Small Vessel Disease.* Front Neurol, 2021. **12**: p. 608797.
41. Pokhilko, A., et al., *Global proteomic analysis of extracellular matrix in mouse and human brain highlights relevance to cerebrovascular disease.* J Cereb Blood Flow Metab, 2021. **41**(9): p. 2423-2438.
42. Al-Thani, M., et al., *A novel human iPSC model of COL4A1/A2 small vessel disease unveils a key pathogenic role of matrix metalloproteinases.* Stem Cell Reports, 2023. **18**(12): p. 2386-2399.
43. Sugiyama, T. and H. Nishitoh, *Neurodegenerative diseases associated with the disruption of proteostasis and their therapeutic strategies using chemical chaperones.* J Biochem, 2024. **176**(3): p. 179-186.

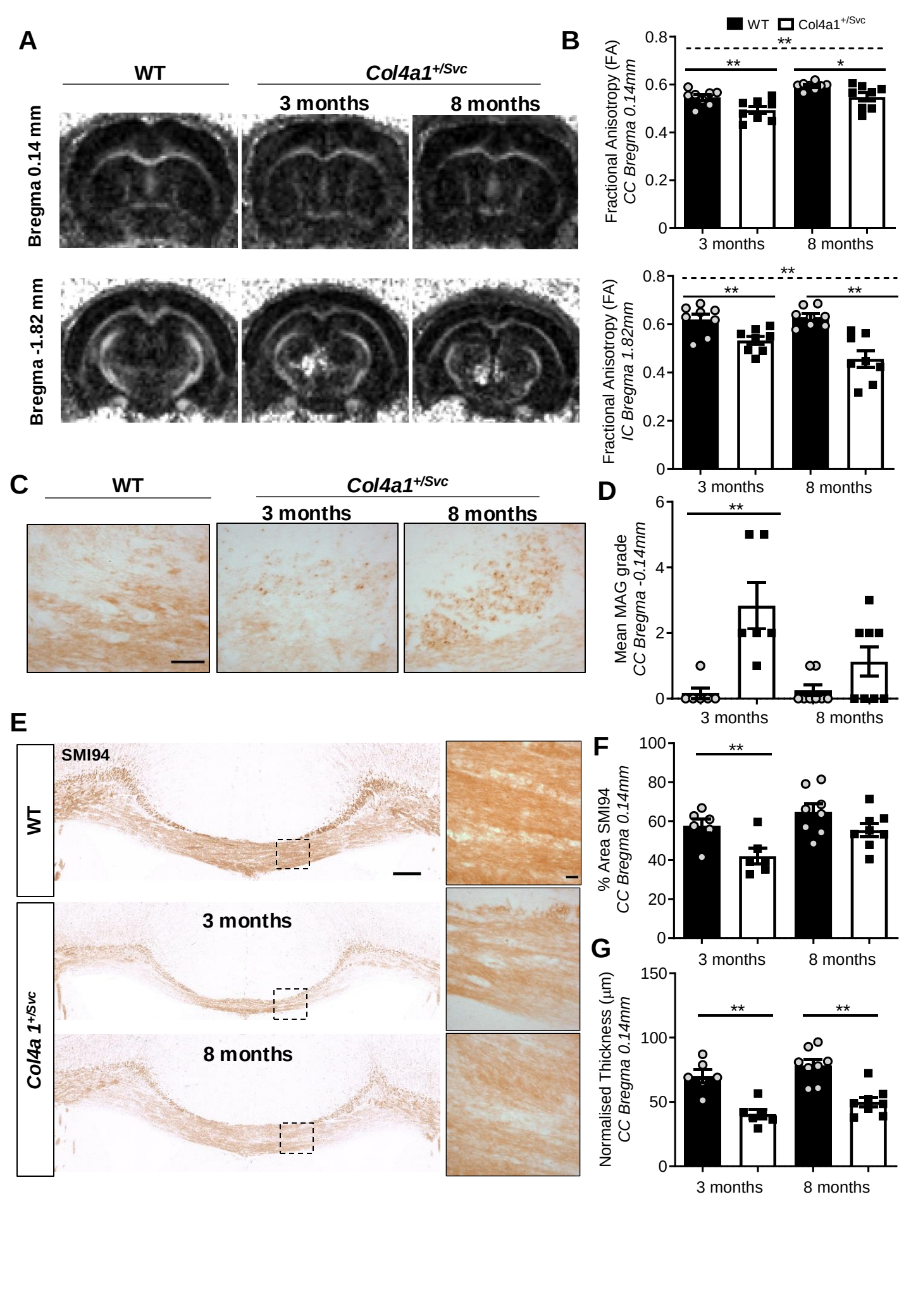
A
WT
Col4a1+/Svc
3 months
8 months
Bregma 0.14 mm
Bregma -1.82 mm
B
WT
Col4a1+/Svc
Fractional Anisotropy (FA)
CC Bregma 0.14mm
Fractional Anisotropy (FA)
IC Bregma 1.82mm
3 months
8 months
C
D
Mean MAG grade
CC Bregma -0.14mm
E
SMI94
WT
Col4a 1+/Svc
F
% Area SMI94
CC Bregma 0.14mm
G
Normalised Thickness (µm)
CC Bregma 0.14mm

Figure 1. White matter abnormalities in *Col4a1*$^{+/Svc}$ mice.
(A) Representative MR-DTI (FA) images from wild type (WT) and *Col4a1*$^{+/Svc}$ mice at 3 and 8 months of age. (B) Quantification of FA values in corpus callosum (CC) and internal capsule (IC) shows Col4a1$^{+/Svc}$ have significantly lower FA values compared to WT-littermates. (C) Representative images of MAG staining (indicative of axon-glial damage) in CC from WT and *Col4a1*$^{+/Svc}$ mice at 3 and 8 month of age. (D) Semi-quantitative grading in CC (Bregma 0.14mm) of MAG staining reveals accumulation of myelin debris and vacuolation, suggesting disruption of axon-glial integrity in *Col4a1*$^{+/Svc}$ mice. (E) Representative images of SMI94 staining in corpus callosum (Bregma level 0.14mm) from WT and *Col4a1*$^{+/Svc}$ animals at 3 and 8 month of age (F) Assessment of SMI94 % area coverage reveals decreased SMI94 density in *Col4a1*$^{+/Svc}$ compared to WT mice. (G) Normalised CC thickness by brain area. Quantification of CC thickness (Bregma level 0.14mm) indicates thinning of corpus callosum in *Col4a1*$^{+/Svc}$ compared to WT mice at both ages. Scale bar (C) 50 µm (E) 100um (E insert) 20 µm. Data analysed by two-way mixed measures ANOVA with post hoc Bonferroni correction (B), by Mann Whitney U (D) or two-way ANOVA (F,G). *$p<0.05$, **$p<0.01$

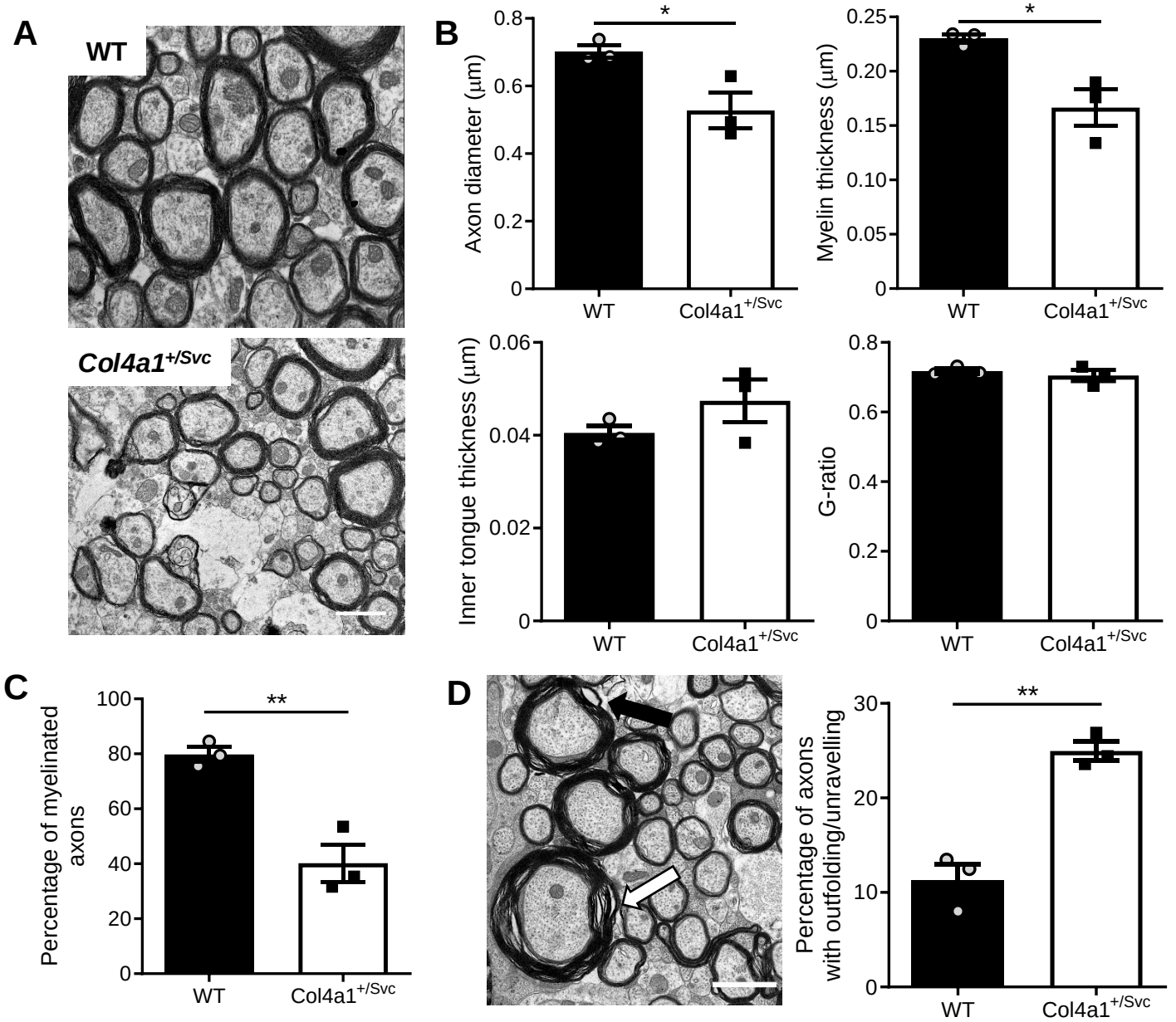

Figure 2. Ultrastructural evidence of axonal and myelin defects.
(A) Representative images of myelinated and unmyelinated axons in CC (Bregma level 0.14mm) from WT and *Col4a1*$^{+/Svc}$ animals. (B) Quantification of axon diameter, myelin thickness, inner tongue thickness and G-ratio. *Col4a1*$^{+/Svc}$ animals have significantly smaller axons with decreased myelin thickness. (C) Quantification of myelinated vs unmyelinated axons in WT and *Col4a1*$^{+/Svc}$ mice. *Col4a1*$^{+/Svc}$ animals have significantly fewer myelinated axons compared to WT. (D) Abnormal phenotypes were identified as outfoldings (black arrow) or unravelling of myelin sheaths (white arrow). Quantification of these indicated that *Col4a1*$^{+/Svc}$ animals have a significantly higher percentage of outfoldings/unravelling compared to WT. Data analysed by t-test. *$p<0.05$, **$p<0.01$. Scale bar 1 µm (A,D).

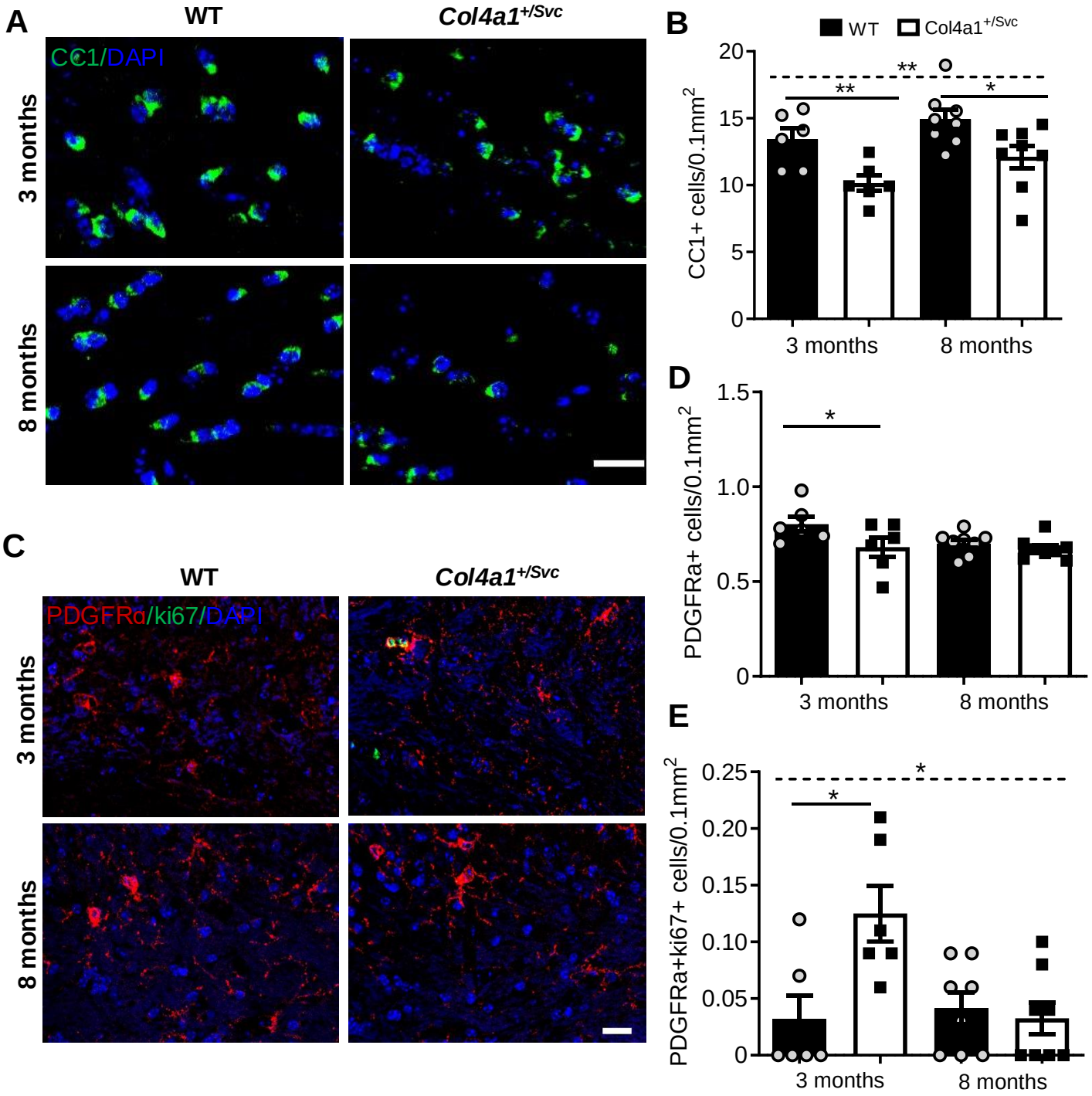

Figure 3. Mature myelinating oligodendrocytes are reduced in *Col4a1*$^{+/Svc}$ mice.
(A) Representative images of CC1+ staining of mature oligodendrocytes in the corpus callosum (CC) (Bregma level 0.14mm) in *Col4a1*$^{+/Svc}$ and WT animals, at 3 and 8 month of age. (B) Quantification of number of mature oligodendrocytes (CC1+) reveals decreased oligodendrocyte numbers in *Col4a1*$^{+/Svc}$ compared to WT mice at 3 and 8 months of age. (C) Representative images of PDGFRα staining for oligodendrocyte precursor cells (OPC) and Ki67 staining for proliferating cells in CC (Bregma level 0.14mm) from WT and *Col4a1*$^{+/Svc}$ animals at 3 and 8 months of age. (D) Quantification of the number of OPC (PDGFRα+) in 3 and 8 months animals indicates a modest decrease in OPCs at 3 months of age, but no differences across genotypes at 8 months of age. (E) Quantification of number of proliferating OPCs (PDGFRα+/Ki67+) in 3 and 8 month mice showed increased proliferation of OPCs in 3 month *Col4a1*$^{+/Svc}$ compared to WT mice. Data analysed by two-way ANOVA *p<0.05, **p<0.01. Scale bar 20 µm.

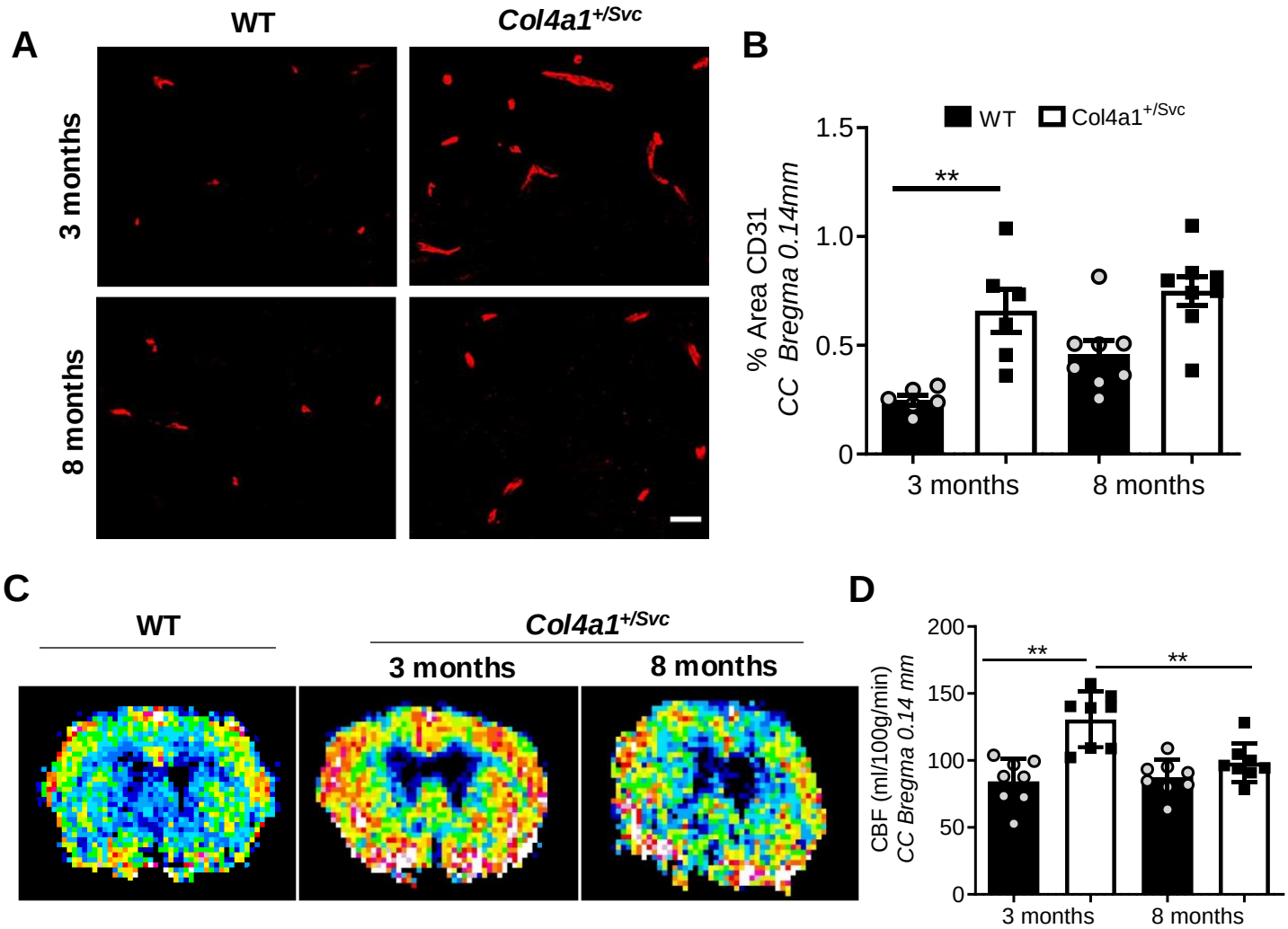

Figure 4. Increased endothelial cell density and perfusion in corpus callosum in *Col4a1*$^{+/Svc}$ mice.
(A, B) Assessment of percentage area CD31 reveals increased CD31 density in *Col4a1*$^{+/Svc}$ mice compared to WT littermates (C) Representative MR Arterial Spin Labelling (ASL) images from WT and *Col4a1*$^{+/Svc}$ animals at Bregma level 0.14mm-0.66mm at 3 and 8 months of age. (D) Quantification of ASL values across genotype and age show that *Col4a1*$^{+/Svc}$ mice have regional differences in CBF. Notably in some regions like the CC, there is a significantly higher perfusion values compared to WT-littermates at 3 and 8 months of age. Data analysed by two-way ANOVA (A, B) or two-way mixed measures ANOVA with post hoc Bonferroni correction **$p<0.01$. Scale bar 20 µm.

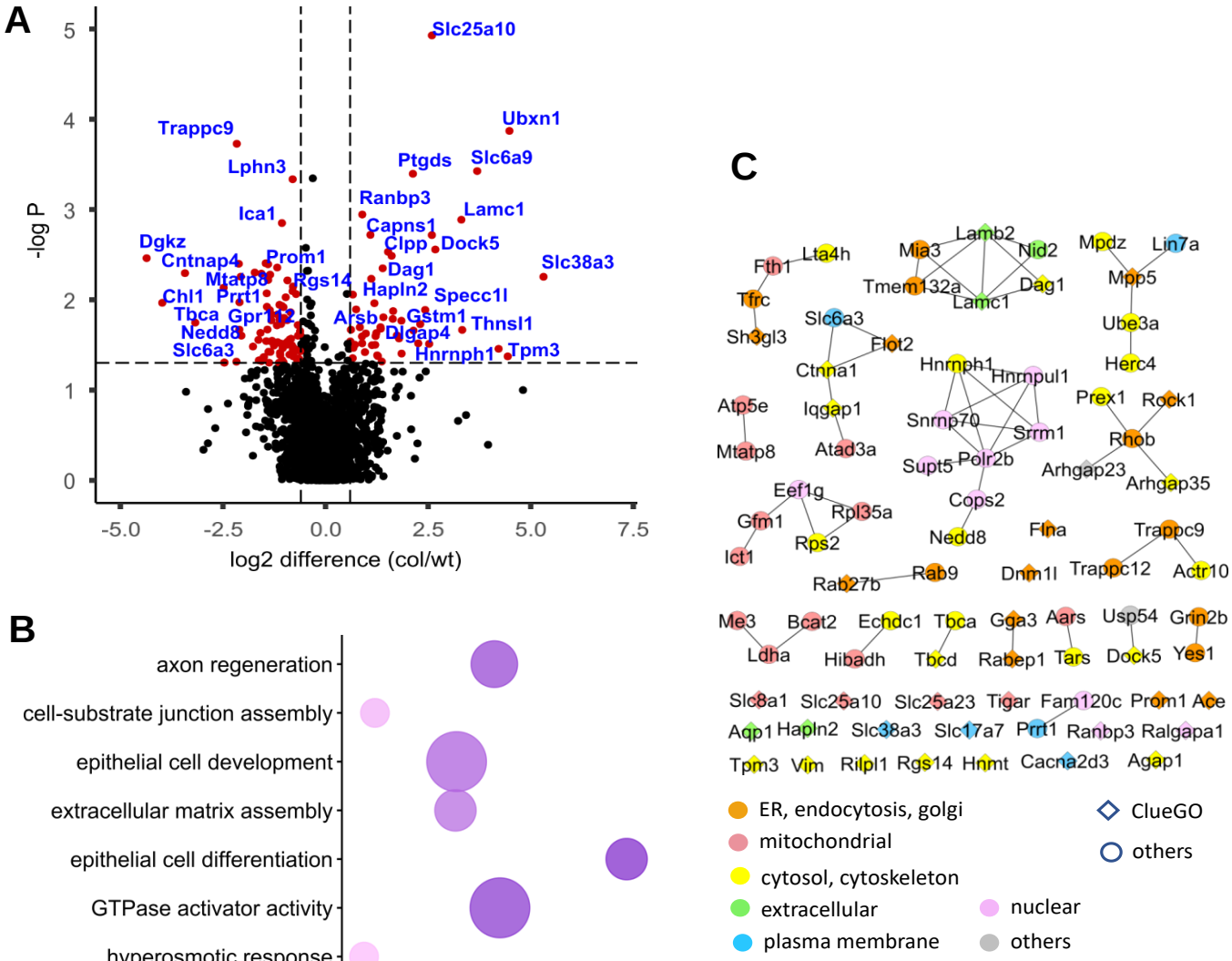

Figure 5. Proteomic investigations highlight white matter proteins and pathways/networks altered in *Col4a1*$^{+/Svc}$ mice.

(A) Volcano plot of differentially regulated proteins between WT and *Col4a1*$^{+/Svc}$ mice, based on all proteins identified in at least 3 biological replicates in each group. Proteins that are present at significantly different levels ($P \leq 0.05$) are marked red with identification in blue. (B) Biological pathways, significantly associated with *Col4a1* mutation (FDR ≤ 0.05), using KEGG and GO BP databases. The analysis was done on differentially regulated proteins from A, using ClueGO plug-in in Cytoscape. Darker colours of the pathway terms corresponds to higher significance. (C) Network of interactions of differentially regulated proteins between WT and *Col4a1*$^{+/Svc}$ mice. The networks were built using the STRING database with a high confidence of interactions. The symbol colours indicate potential location of the protein, predicted based on String location score as described in Methods. The shape of the symbols shows whether the protein is also present in the pathway terms from ClueGO analysis.

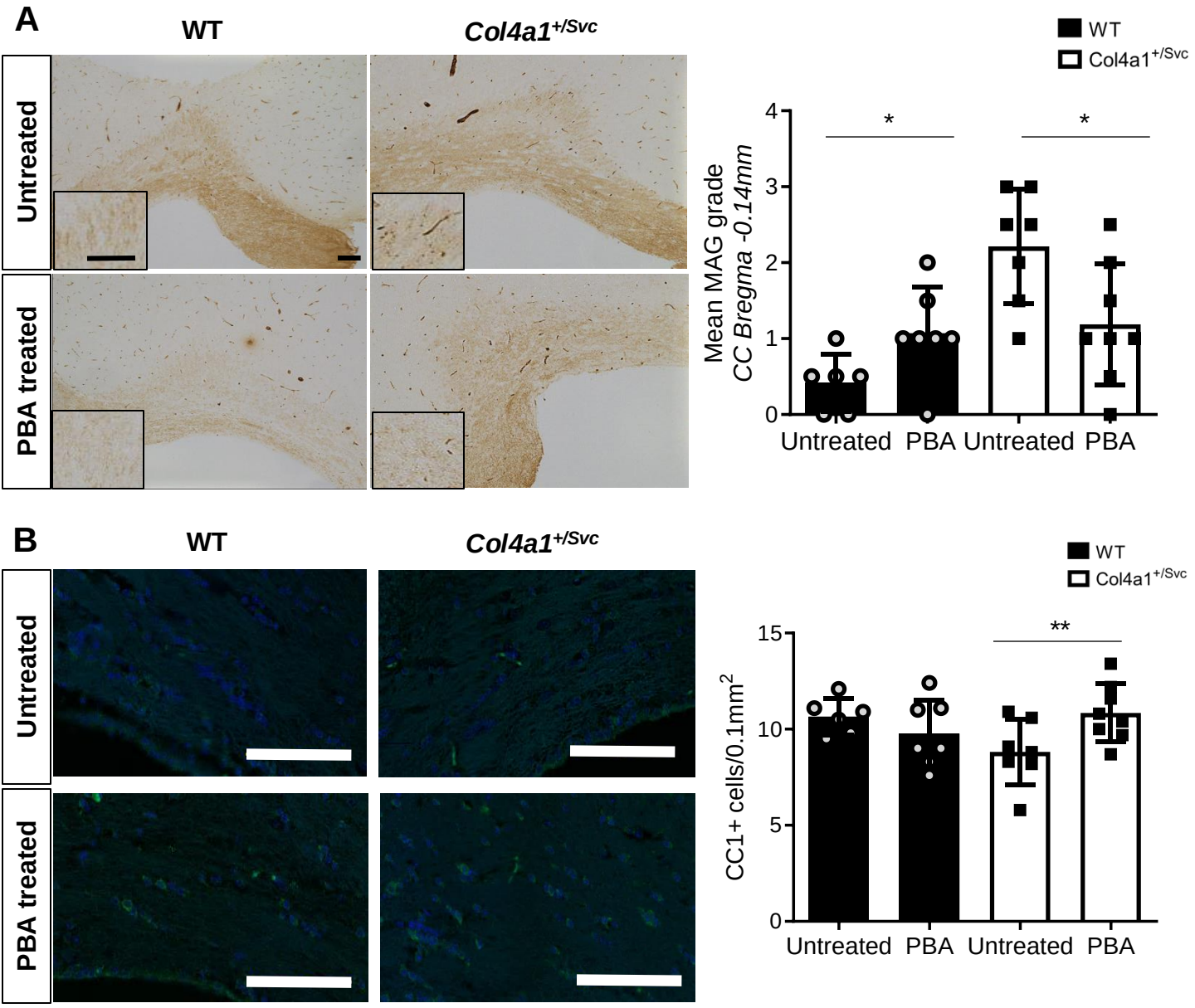

Figure 6. PBA treatment promotes white matter integrity and myelinating oligodendrocytes in *Col4a1*$^{+/Svc}$ mice.

(A) Representative images of MAG immunostaining in corpus callosum in PBA-treated and untreated WT and *Col4a1*$^{+/Svc}$ mice. (Scale bars= 50µm). Grading of myelin debris accumulation highlights a significant accumulation of myelin debris in the *Col4a1*$^{+/Svc}$ mice compared to PBA-treated *Col4a1*$^{+/Svc}$ mice. PBA treatment also increased myelin debris in WT mice. Data analysed by Mann Whitney U. (B) Representative images of CC1 staining of mature oligodendrocytes in corpus callosum in *Col4a1*$^{+/Svc}$ and WT animals. (Scale bar= 100µm). Quantification of number of mature oligodendrocytes (CC1+ve) reveals increased oligodendrocyte numbers in PBA treated *Col4a1*$^{+/Svc}$ compared to untreated mice. Data analysed by two-way ANOVA with Tukey multiple comparisons tests (untreated WT/*Col4a1*$^{+/Svc}$, n=6/7; PBA treated WT/*Col4a1*$^{+/Svc}$, n=7/8 $^{**}p<0.01$).

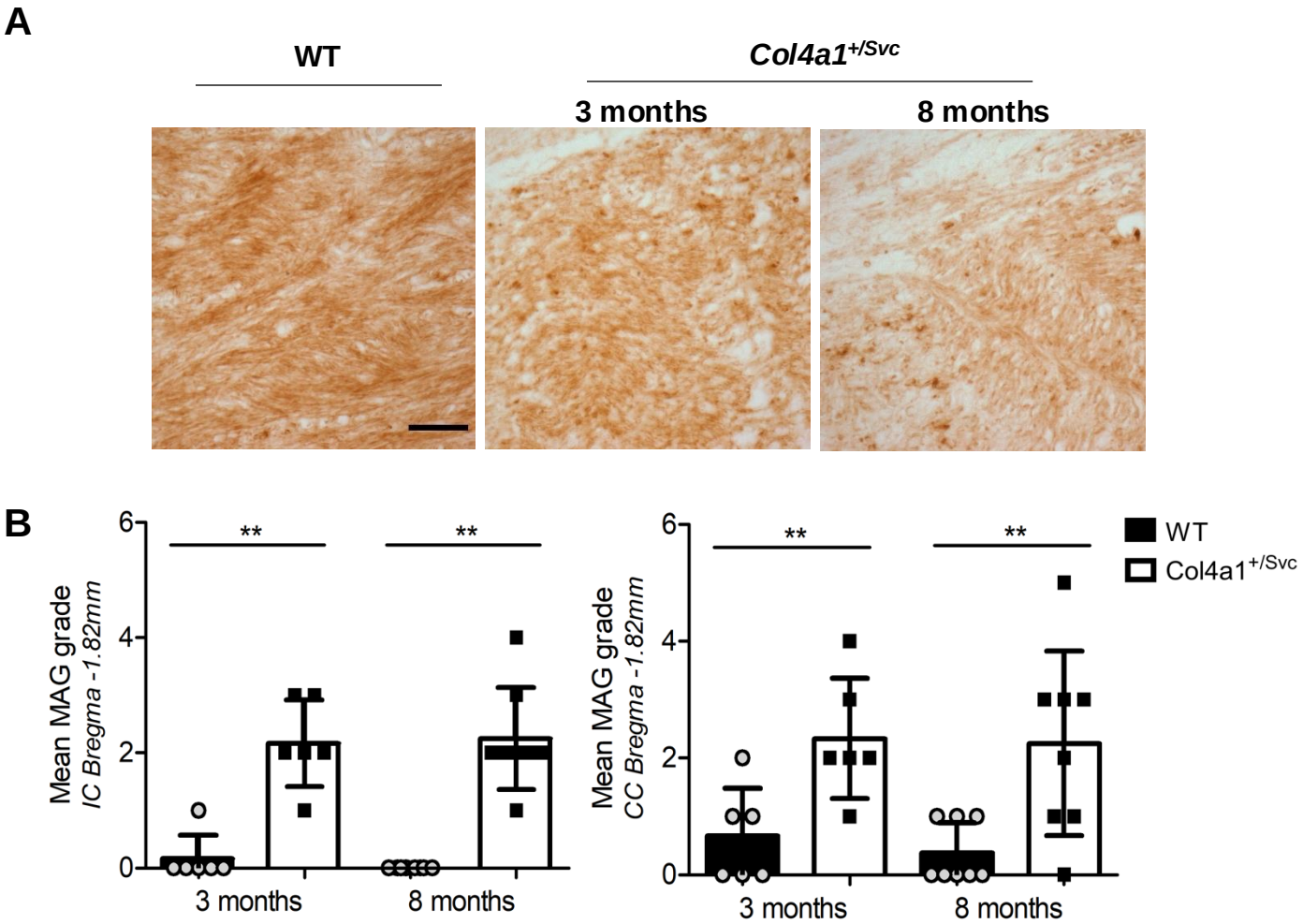

Supplementary Figure 1. Axon-glial damage in *Col4a1*$^{+/Svc}$ mice.
(A) Representative images of MAG staining (indicative of axon-glial damage) in internal capsule (IC) from WT and *Col4a1*$^{+/Svc}$ mice at 3 and 8 month of age. (B) Semi-quantitative grading in IC and CC (Bregma -1.82mm) of MAG staining reveals accumulation of myelin debris and vacuolation, suggesting disruption of axon-glial integrity in *Col4a1*$^{+/Svc}$ mice. Data analysed by Mann Whitney U. *p<0.05, **p<0.01. Scale bar = 20µm

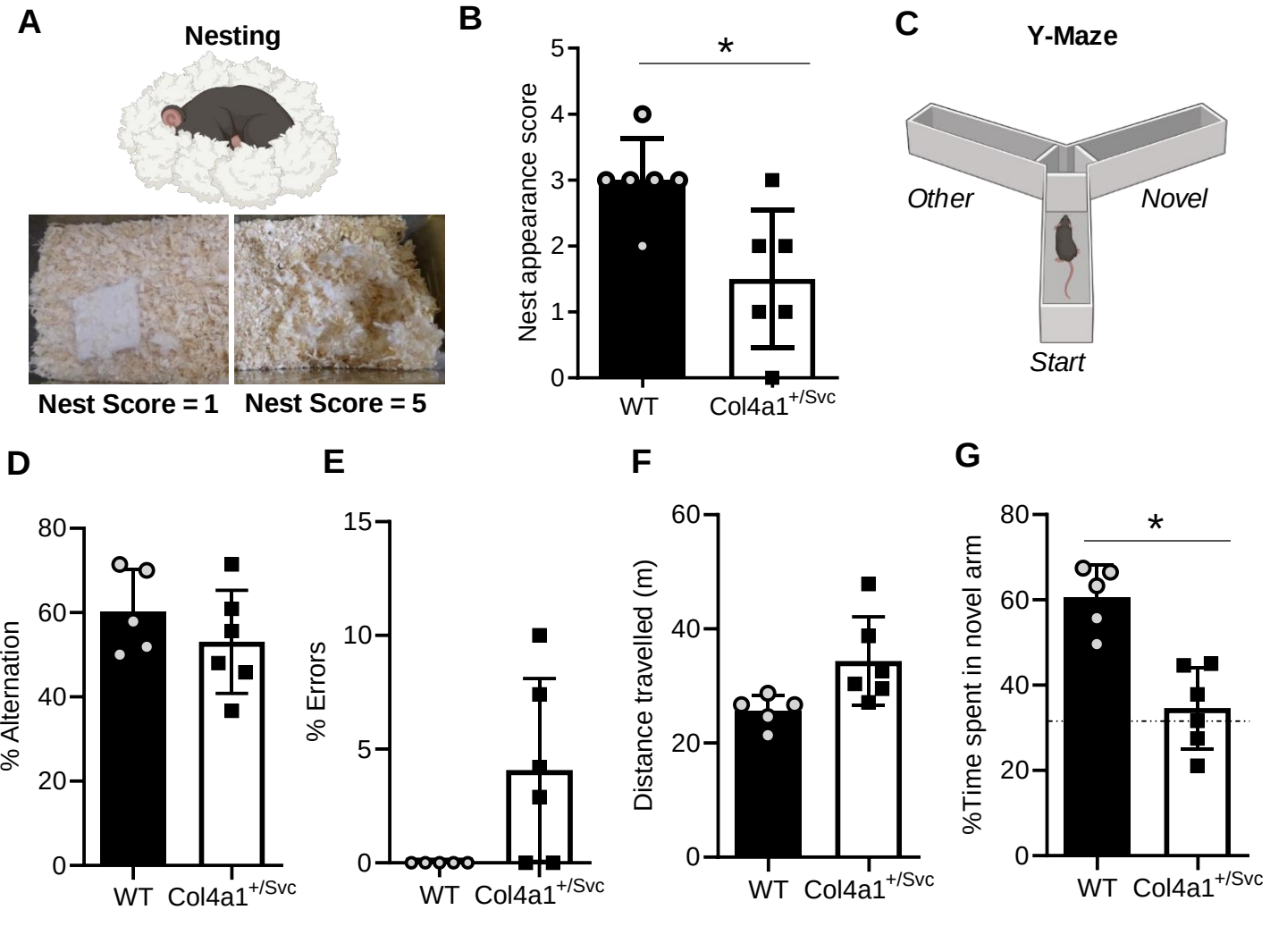

Supplementary Figure 2. Cognitive and executive brain function is impaired in *Col4a1$^{+/Svc}$* mice.
(A) Nesting apparatus. Nesting ability was scored on appearance of nests and representative images of nests with score of 1 and 5 respectively are shown. (B) Quantification of nesting ability (in *Col4a1$^{+/Svc}$* animals and WT littermates at 8 months of age. Col4a1$^{+/Svc}$ mutants show decreased nesting ability, indicative of impaired executive function. (C) Y-Maze apparatus. (D) Percent spontaneous alternation between 3 arms of Y-maze in WT and *Col4a1$^{+/Svc}$* mice were not significantly different. (E) Percent errors during spontaneous alternation in WT and *Col4a1$^{+/Svc}$* mice indicates *Col4a1$^{+/Svc}$* tend to make more errors than WT mice. (F) Total distance travelled during the spontaneous alternation task was not significantly different in WT and *Col4a1$^{+/Svc}$* mice. (G) Percent time WT and *Col4a1$^{+/Svc}$* mice spent exploring the novel arm during retention phase were significantly different with *Col4a1$^{+/Svc}$* mice spending less time exploring the novel arm compared to the WT. WT/*Col4a1$^{+/Svc}$*; n=5/6, Mann-Whitney U tests were used for statistical analyses. Measures are presented as a mean ±SE. * $p<0.05$). Dotted line represents chance level.